https://doi.org/10.5194/egusphere-2026-4149
Preprint. Discussion started: 15 September 2026

Snow–Ice Morphological Relationship under Sea Ice Surface Topographic Control: Evidence from In Situ RTK Measurements

Mingfeng Wang[1, 2], Jie Su[1, 2, 3], Hao Li[1, 2] and Tao Li[1, 2, 3]

[1] Frontier Science Center for Deep Ocean Multispheres and Earth System (FDOMES) and State Key Laboratory of Physical Oceanography, Ocean University of China, Qingdao, China
[2] Key Laboratory of Transparent Arctic, Ocean University of China, 5 Yushan Rd, Shinan District, Qingdao, Shandong, 266005, China
[3] Laboratory for Ocean Dynamics and Climate, Qingdao Marine Science and Technology Center, Qingdao, Shandong, 266237, China

Correspondence to: Jie Su (sujie@ouc.edu.cn)

Abstract. Sea ice surface roughness plays a critical role in snow redistribution and accumulation; however, the spatial scale at which its influence is most effective remains poorly constrained by field observations. During the 15th Chinese National Arctic Research Expedition in 2025, synchronous measurements of ice surface elevation and snow depth were conducted using a lightweight Global Navigation Satellite System (GNSS) Real-Time Kinematic (RTK) system. Observations were collected over multi-year sea ice in the central Arctic north of 85°N, encompassing both level ice and deformed ice regimes. Multi-scale moving-window analysis revealed a strong scale dependence in the statistical relationship between sea ice surface roughness and mean snow depth. The ensemble-mean correlation coefficient reached a maximum at a window radius of approximately 7–10 m ($r \approx 0.56$), indicating that this scale dominates the coupling between surface roughness and snow redistribution. At this characteristic scale, rougher ice surfaces generally corresponded to greater snow depths, reflecting the enhanced trapping and retention of wind-blown snow by complex surface topography during wind-driven transport. These findings provide observational constraints for parameterizing snow redistribution processes on sea ice and offer guidance for selecting appropriate spatial resolutions in remote-sensing products aimed at resolving roughness-controlled snow processes.

1 Introduction

Sea ice and its overlying snow cover play a crucial role in the Arctic climate system by modulating air–sea heat exchange, controlling surface albedo, and influencing the timing of melt onset (Sturm et al., 2002; Webster et al., 2014; Itkin et al., 2017). The spatial distribution of snow depth over sea ice is highly heterogeneous, governed by snowfall input, wind-driven redistribution, ice deformation processes, and thermodynamic evolution. For instance, snow tends to accumulate on the leeward sides of ridges and other deformed ice features, leading to pronounced contrasts in snow distribution between level ice and rough ice (Merkouriadi et al., 2020; Itkin et al., 2023). Field observations consistently show deeper snow in ridged and deformed ice areas, whereas snow over smooth, undeformed first-year ice is typically thinner and more uniform (King et

https://doi.org/10.5194/egusphere-2026-4149
Preprint. Discussion started: 15 September 2026

al., 2018; Nandan et al., 2023). This redistribution pattern directly links snow depth to surface roughness, highlighting the need to better quantify the snow depth–roughness relationship.

However, studying the snow depth–roughness relationship using satellite remote sensing remains challenging. Snow depth retrievals, whether derived from passive microwave, active microwave radar, or laser altimetry, have been shown to be highly sensitive to surface roughness across multiple scales, ranging from radar wavelengths to floe-scale features such as ridges and leads (King et al., 2018; Nab et al., 2023). Consequently, relationships derived from remote sensing data often reflect signal perturbations induced by roughness rather than the underlying physical mechanisms of snow redistribution. This issue also introduces systematic uncertainties in satellite altimetry-based sea ice thickness retrievals (Landy et al., 2020).

Field campaigns play an indispensable role in advancing observations of snow depth and sea ice surface roughness. For example, coordinated observations during the BROMEX (2012) and Eureka (2014) campaigns provided high-resolution in situ datasets for evaluating Operation IceBridge (OIB) radar-derived snow depth products (Webster et al., 2014; King et al., 2015; Kwok et al., 2017). These studies revealed strong correlations between snow depth variability and surface roughness and found that the spatial correlation length scale of snow depth can be as short as 5–7 m, much smaller than the footprint of airborne or satellite sensors (Kwok et al., 2017). This implies that even minor geolocation mismatches caused by ice drift between airborne and ground observations may introduce significant biases in rough ice regions, where snow depth varies sharply (Sturm et al., 2006). For this reason, previous campaigns were typically conducted over landfast ice to minimize spatial mismatches due to ice motion. However, landfast ice represents only a limited portion of the Arctic sea ice cover and differs substantially from drifting ice in both dynamic and thermodynamic conditions. Therefore, high-resolution in situ observations over drifting sea ice are still needed.

The 15th Chinese National Arctic Research Expedition provided an opportunity to explore new observational approaches. During this campaign, a high-precision Global Navigation Satellite System（GNSS）-based elevation measurement system was systematically deployed at multiple Arctic sea ice stations. By integrating Post-Processing Kinematic (PPK)/ real-time kinematic (RTK) positioning systems with snow probes, a comprehensive observation framework at the station scale was established. A fixed base station was installed on drifting ice, enabling real-time kinematic (RTK) positioning within a reference frame moving with the ice. This setup allows centimeter-level measurements of ice surface elevation, while snow probes provide elevation data for both the snow surface and the snow–ice interface, forming a consistent dataset of ice freeboard and snow depth. To address spatial mismatches caused by continuous ice drift, the RTK measurements were conducted within an ice-fixed reference frame, ensuring temporal and spatial consistency among different observations. Using high-resolution RTK transect data collected over multi-year ice during the 2025 expedition, this study focuses on: (1) developing an integrated RTK-based in situ observation system for sea ice interface elevations; (2) examining the geometric consistency between ice surface and snow surface elevations; (3) identifying the characteristic spatial scale of ice surface roughness; (4) determining the optimal coupling scale at which surface roughness modulates snow depth. By explicitly quantifying the scale dependence of the roughness–snow depth relationship, this study aims to provide observational

https://doi.org/10.5194/egusphere-2026-4149
Preprint. Discussion started: 15 September 2026

constraints for parameterizing snow redistribution processes over sea ice and to inform the design of spatial resolution in remote sensing retrieval products.

2 Observations and Data Processing

2.1 Instrumentation

This study employs a lightweight GNSS RTK positioning system for in situ measurements of sea ice and snow surface elevation anomalies, as well as snow depth. The system adopts an integrated design, combining the GNSS receiver, antenna, communication module, and power supply into a single compact unit (Fig. 1). Its small size facilitates transportation, deployment, and mobile measurements in sea ice environments. In terms of positioning capability, the system supports multi-constellation and multi-frequency GNSS observations, including BeiDou, GPS, GLONASS, and Galileo. This ensures stable satellite availability and reliable differential positioning performance in high-latitude regions. Under RTK mode, the system can achieve millimeter-level accuracy in both horizontal and vertical positioning, meeting the precision requirements for measuring ice surface elevation as well as snow surface and snow–ice interface elevations.

The system supports both base station and rover operating modes. In this study, one RTK unit was deployed as a fixed base station on a stable ice surface, drifting with the ice（Fig.1), continuously collecting GNSS data and broadcasting differential correction signals to the rover via wireless communication. Meanwhile, a second RTK unit operated as a rover, conducting elevation measurements of the ice surface and snow interfaces within the coverage area of the base station（Fig.1）. Observations were carried out using RTK positioning by installing a base station on drifting sea ice to establish a quasi-stationary local reference frame relative to the ice surface. Within this reference frame, differential positioning between the base and rover effectively removes the influence of bulk ice translation and rotation on the positioning results, allowing the retrieved elevations to represent the true geometric variations relative to the ice surface. This approach provides an effective solution to the spatial mismatch problem caused by continuous ice drift and ensures the spatial and temporal consistency of different observational variables.

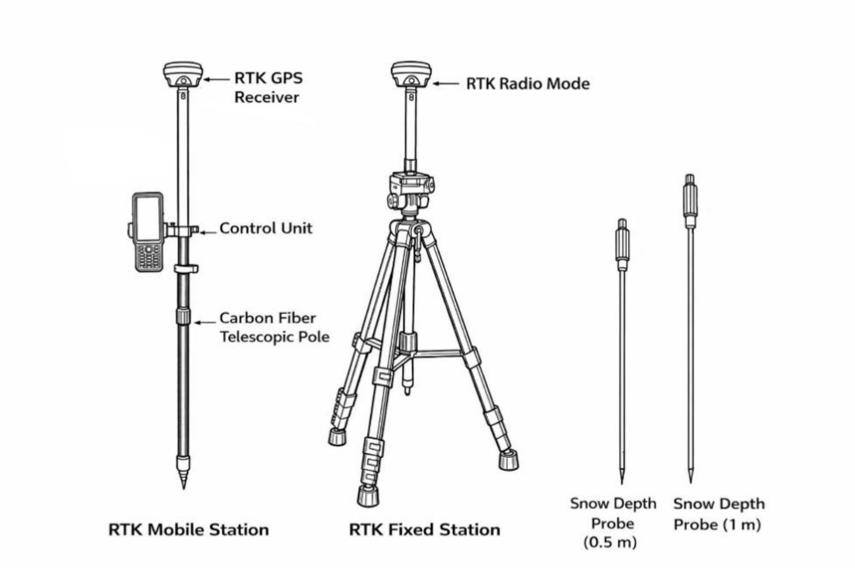

Figure 1. Schematic of the snow depth observation system and measurement instruments. The left panel shows the RTK rover, the middle panel shows the RTK base station, and the right panel shows snow depth probes of different lengths (0.5 m and 1 m).

To accommodate varying snow depths, snow probes of 0.5 m and 1 m length were used under different snow conditions and were rigidly mounted to the RTK rover during measurements. The probe features a pointed tip at its lower end; by making contact with the snow surface, it enables precise determination of the snow surface elevation. The probe is then inserted vertically into the snow at the same location. When further penetration is no longer possible, this position is assumed to correspond to the snow–ice interface, and the corresponding elevation is recorded as the ice surface elevation. Snow depth is thus directly obtained as the elevation difference between the snow surface and the snow–ice interface measured at the same point.

The snow surface is clearly distinguishable, allowing the pointed probe to accurately determine the snow surface elevation upon contact. After measuring the snow surface elevation, the probe is further inserted at the same location until it reaches the dense ice layer, which is identified by a distinct increase in mechanical resistance. This point is interpreted as the snow–ice interface, and the corresponding elevation provides a stable estimate of the ice surface elevation. The tip angle and diameter, play an important role in determining penetration performance and positional stability during insertion into snow and ice layers. Tests of the probe geometry indicate that a probe with a diameter of 10 mm and a tip angle of 30° provides an optimal balance between penetration capability and positional stability under snow conditions. This configuration enables effective penetration through unconsolidated snow while producing a distinct and repeatable mechanical response upon contact with the ice surface, thereby ensuring reliable identification of the snow–ice interface.

Because both the snow surface and snow–ice interface elevations are measured at the same location within the same reference frame, systematic biases associated with instrument switching or spatial misregistration are effectively avoided,

https://doi.org/10.5194/egusphere-2026-4149
Preprint. Discussion started: 15 September 2026

improving the consistency and reliability of snow depth estimates. In addition, the RTK system used in this study is equipped with an inertial measurement unit (IMU) for tilt compensation. The tilt-compensation capability ensures that the retrieved elevations are not affected by probe inclination during insertion. This capability is particularly important in snow-covered environments, enabling greater operational flexibility and higher observational efficiency without compromising measurement accuracy.

2.2 Field Observations

The field data used in this study were collected during the 15th Chinese National Arctic Research Expedition in 2025 (July 6 – September 26). Observations were conducted in the central Arctic, with the study area located north of 85°N in a region dominated by multi-year ice. The sea ice in this area exhibits well-developed surface morphology, characterized by pronounced roughness and distinct snow redistribution patterns. Based on in situ ice core drilling measurements, the sea ice thickness at the observation sites ranges from 1.2 to 1.8 m, which is representative of typical summer multi-year ice conditions. A total of nine observations were conducted at five ice stations during the campaign, including four short-term stations (nice0201, nice0301–0302, nice0401, and nice0601–0602) and one long-term station (niceL01–niceL03). The short-term stations lasted several hours each, while the long-term station was maintained continuously for 7 days. In total, nine RTK transects were collected. The spatial distribution of these stations is shown in Fig. 2.

https://doi.org/10.5194/egusphere-2026-4149
Preprint. Discussion started: 15 September 2026

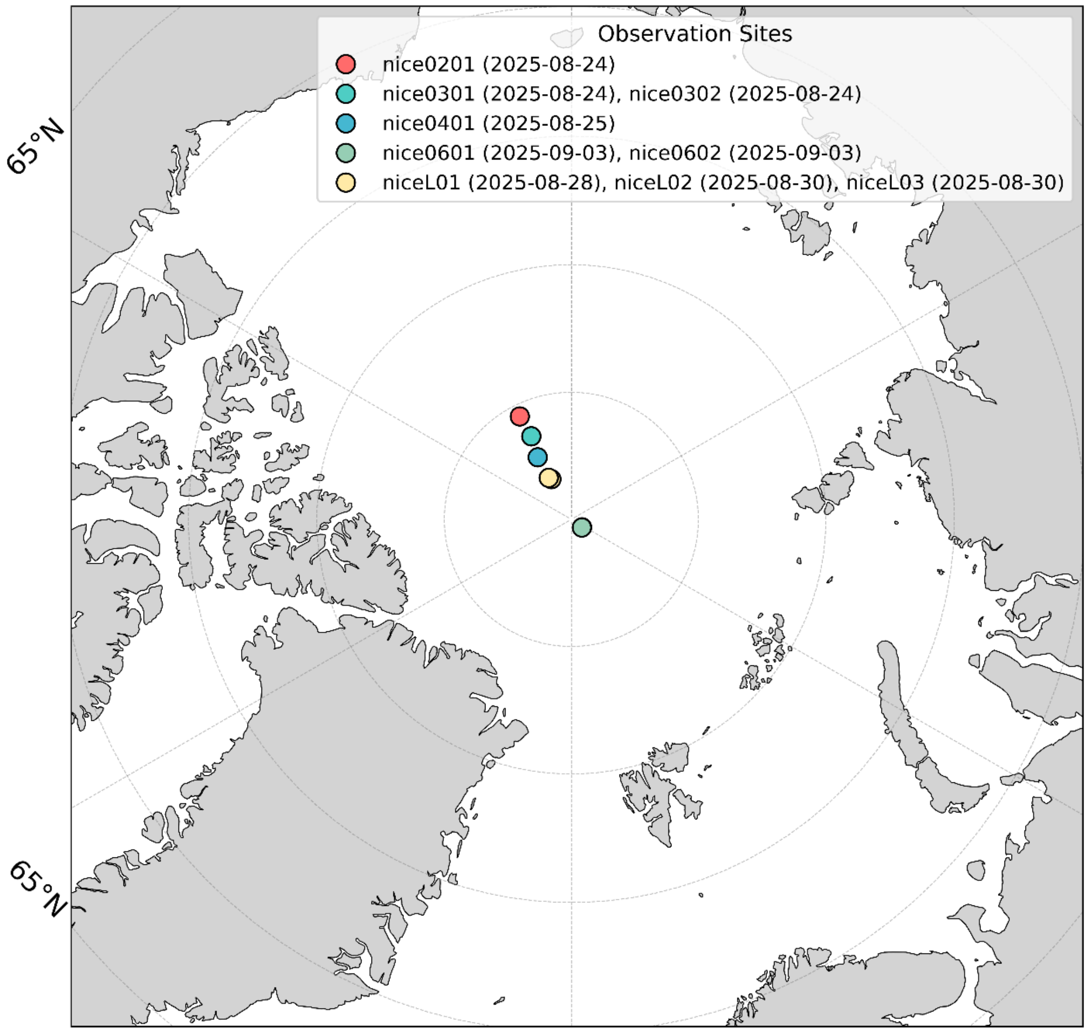

Figure 2. Schematic map showing the spatial distribution of the observation sites.

The operational procedure is as follows:

1). At the beginning of each survey, an RTK base station was installed at a selected stable ice location to ensure secure deployment and proper system initialization. The base station connected to GNSS satellites, establishing a precise reference frame.

2). The RTK rover was then linked to the base station, continuously receiving real-time differential correction signals via the internal radio link. Elevation measurements were initiated once a fixed solution was achieved.

3). At each sampling point, a snow probe of known length was first brought into contact with the snow surface to record the snow surface elevation. The probe was then inserted vertically at the same location until reaching the snow–ice interface,

https://doi.org/10.5194/egusphere-2026-4149
Preprint. Discussion started: 15 September 2026

where the corresponding elevation was recorded. The difference between these two measurements was used to compute snow depth.

An overview of the field observations is shown in Fig. 3.

Figure 3. (a) The research vessel Xuelong 2 at the long-term ice station. (b) Deployment of the survey transect by field personnel. (c) Initialization of measurement equipment. (d) Measurement points recorded after completion of field observations. Photographs by Chenshuai Wei and Honggen Wang and Jie Su.

At each ice station, RTK survey transects were designed along representative directions to obtain continuous, high-precision elevation measurements of both the ice surface and the snow surface. Transects typically extended from relatively level ice areas to ridges and their slopes, thereby capturing a range of surface morphologies and spatial scales. A non-uniform sampling strategy was adopted: over level ice, where elevation and snow depth variability are small, sampling intervals were relatively large; in contrast, over ridges and slopes, where snow depth variability is significant and closely linked to ice surface elevation, higher sampling density was used to ensure sufficient representation across different snow depth regimes.

https://doi.org/10.5194/egusphere-2026-4149
Preprint. Discussion started: 15 September 2026

The spatial distribution, length, and sampling density of each transect are shown in Fig. 4. Transects are displayed in a local planar coordinate system, with transect lengths and geometries varying considerably, reflecting differences in site conditions, surface morphology, and accessibility constraints.

The total observation transect length was 1.84 km, of which 1.47 km remained after quality control and screening of valid measurement points. Some stations feature relatively short transects (~22–34 m), whereas others (e.g., nice0401, nice0601, nice0602, niceL01) extend over hundreds of meters, providing more robust sampling for multi-scale statistical analysis. The number of sampling points per transect ranges from 22 to 82, with point spacing between 0.5 m and 4 m, and total transect lengths ranging from approximately 22 to 729 m. Overall, more than one thousand paired observations of ice surface elevation and snow interface elevations were collected across multiple sea ice stations.

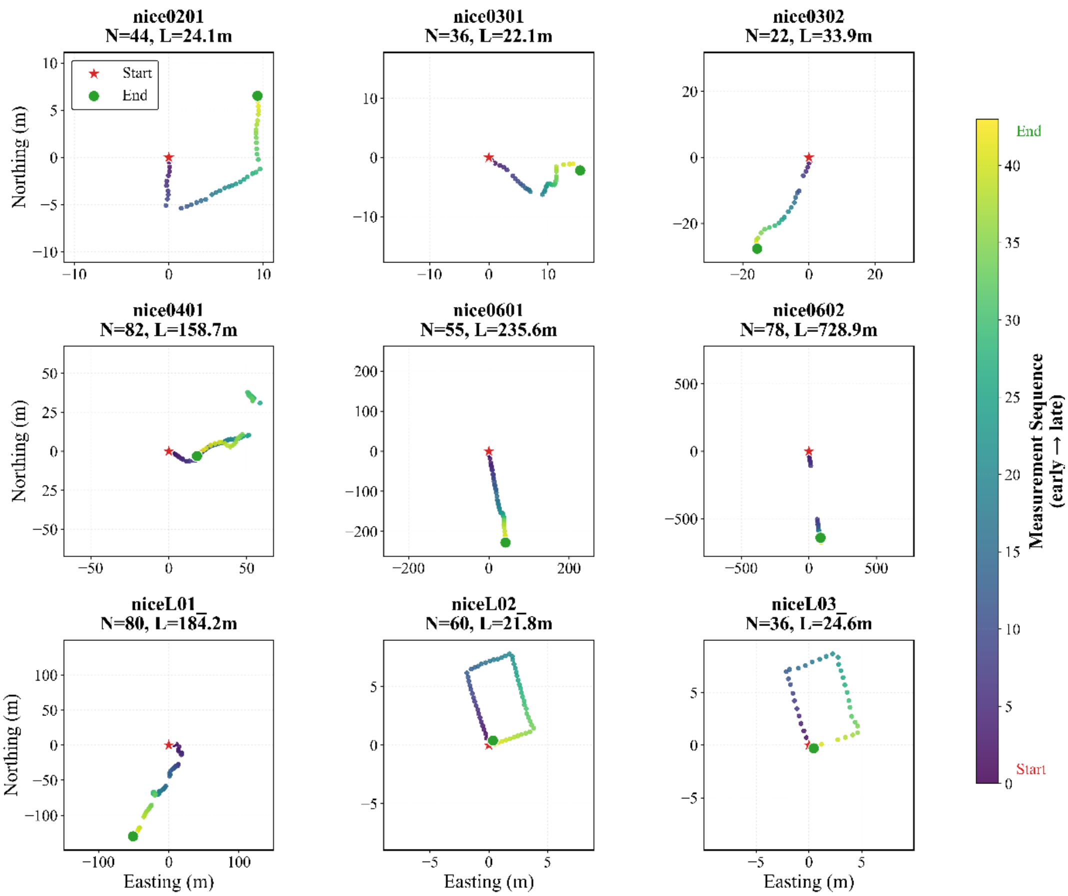

Figure 4. Spatial distribution of RTK survey transects at each ice station. Red stars marking the starting points and green circles indicating endpoints. The color of the points transitions from purple to yellow, representing the temporal sequence of measurements from early to late.

https://doi.org/10.5194/egusphere-2026-4149
Preprint. Discussion started: 15 September 2026

2.3 Data Processing

1) Spatial Pairing and Quality Control

RTK observations were recorded sequentially as point-based measurements containing geographic coordinates and elevation, with consecutive records representing the same location due to the "two measurements at one location" snow depth measurement approach. Therefore, the first step in data processing involves spatial pairing and quality control. Horizontal distances between consecutive records were computed using the Haversine formula. When the horizontal distance between two consecutive records was less than 0.1 m, they were considered to represent the same sampling point and grouped into a single observation pair. This threshold is much smaller than the spacing between adjacent sampling points (0.5–4 m), ensuring reliable discrimination between distinct points and repeated measurements at the same location. For each observation group, only pairs containing exactly two elevation records were retained. The higher elevation was defined as the snow surface, and the lower elevation as the snow–ice interface. The geographic coordinates of the point were taken as the average of the two measurements to reduce random positioning errors. Groups that did not meet these criteria (e.g., single measurements or more than two records) were discarded.

2)Elevation Profile Smoothing and Snow Depth Calculation

To reduce high-frequency noise inherent in field measurements while preserving the true morphological variability along transects, Savitzky–Golay filtering was applied separately to the snow surface and ice surface elevation profiles. This method, widely used in topographic, ice-sheet, snow-depth, and DEM analyses, performs a local polynomial least-squares fit within a moving window, effectively smoothing noise without significantly altering slope and curvature. A second-order polynomial with a window size of five points was adopted, balancing noise suppression and feature preservation.

To facilitate comparison across transects and eliminate differences in absolute elevation reference, elevations were normalized by subtracting the mean ice surface elevation, yielding relative elevation profiles that emphasize along-track variability (Fig. 5). Snow depth was defined as the elevation difference between the snow surface and the snow–ice interface at each sampling point. Based on the smoothed elevation profiles, snow depth was computed point by point (Fig. 6).

https://doi.org/10.5194/egusphere-2026-4149
Preprint. Discussion started: 15 September 2026

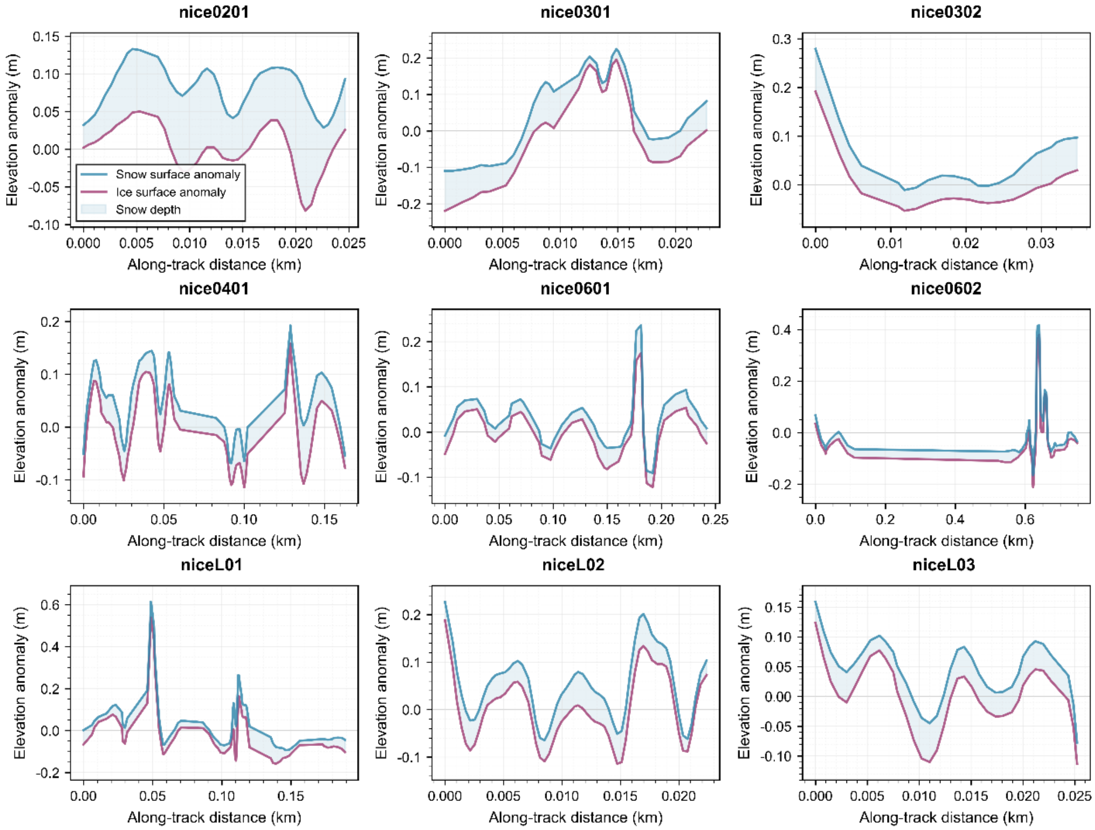

185 **Figure 5. Along-track distributions of ice surface and snow surface elevation anomalies for the nine RTK transects. Each panel corresponds to an individual RTK transect (nice0201–niceL03). The x-axis represents along-track distance (km), and the y-axis shows detrended elevation anomalies (m) relative to the mean of each transect. The blue curves denote snow surface elevation anomalies, and the red curves denote ice surface elevation anomalies.**

https://doi.org/10.5194/egusphere-2026-4149
Preprint. Discussion started: 15 September 2026

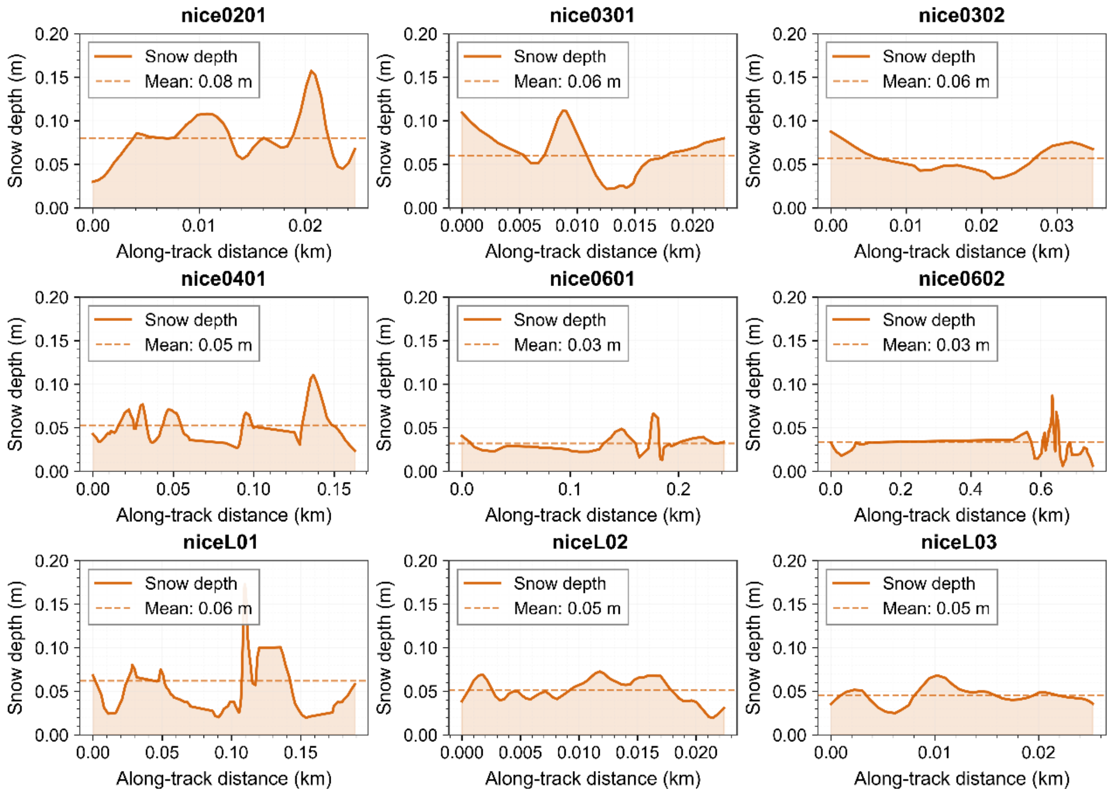

Figure 6. RTK-derived snow depth profiles. The orange curve represents the snow depth, with the semi-transparent orange fill highlighting the spatial distribution of snow cover. The dashed orange line indicates the mean snow depth for each track.

3 Result

3.1 Snow Depth and Ice–Snow Interface Elevations

To quantitatively characterize the morphological features of ice surface and snow surface elevation anomalies along the nine RTK transects, three metrics were employed: the peak-to-valley range (Ice/Snow P–V), the robust amplitude defined as the 95%–5% percentile range (Ice/Snow R–A), and the amplitude ratio (Amp Ratio) (Table 1). The peak-to-valley range is defined as the difference between the maximum and minimum elevation anomalies along a given transect. The robust amplitude is defined as the difference between the 95th and 5th percentiles of the elevation anomaly distribution, which reduces the influence of extreme values. The amplitude ratio is calculated as the ratio of the robust amplitude of the ice surface to that of the snow surface, and is used to quantify the relative magnitude of surface undulations between ice and snow. An amplitude ratio greater than 1 indicates that ice surface variability exceeds that of the snow surface, suggesting a smoothing or infilling effect of the snow layer on the underlying ice topography. Conversely, a ratio less than 1 indicates relatively larger variability in the snow surface, which may be associated with local redistribution or wind-driven accumulation effects. A ratio equal to 1 implies that the snow surface variability directly inherits that of the ice surface. Across all transects, the peak-to-valley range of ice surface elevation anomalies varies from 0.10 to 0.71 m (robust amplitude: 0.093–0.47 m), while snow surface anomalies show nearly identical ranges of 0.13–0.70 m (robust amplitude: 0.11–0.46 m). These comparable magnitudes indicate that snow surface roughness is broadly equivalent to that of the underlying ice. The characteristics and scale dependence of ice surface roughness are discussed further in section 3.2. For most transects, the amplitude ratio between ice and snow surfaces is close to 1, ranging from 0.86 to 1.20. This suggests that, at the along-track scales considered in this study, snow surface morphology tends to reflects the underlying ice topography. Deviations provide further insight: ratios below 0.9 (e.g., 0.86) imply a smoothing effect, likely due to preferential snow accumulation in topographic depressions; conversely, ratios above 1.1 (e.g., 1.20) suggest an amplification effect, potentially caused by enhanced snow deposition over elevated features. Overall, while ice and snow surface elevation variations exhibit strong consistency, the ratio's deviation reveals measurable differences in surface roughness characteristics across transects.

Table I. Track-length-weighted statistics of ice and snow surface roughness and snow depth over different topographic classes derived from RTK profiles.

Track	Length (km)	Ice P-V(m)	Ice R-A	Snow P-V	Snow R-A	Amp Ratio
nice0201	0.02	0.13	0.11	0.10	0.09	1.09
nice0301	0.02	0.42	0.38	0.33	0.32	1.16
nice0302	0.03	0.25	0.17	0.29	0.20	0.82
nice0401	0.16	0.27	0.21	0.26	0.19	1.06
nice0601	0.24	0.30	0.23	0.33	0.26	0.92
nice0602	0.75	0.59	0.46	0.58	0.47	0.96
niceL01	0.19	0.70	0.45	0.71	0.46	0.95
niceL02	0.02	0.30	0.22	0.29	0.24	0.99
niceL03	0.03	0.24	0.18	0.24	0.14	1.11
Mean	**0.16**	**0.46**	**0.34**	**0.46**	**0.35**	**0.97**

Figure 7 further illustrates the correlation between ice surface and snow surface elevation anomalies along the nine RTK transects. The results show that, except for a few short transects, most exhibit a strong linear relationship between ice and snow surface elevation anomalies, with correlation coefficients generally exceeding 0.96 and all passing significance tests (all $p < 0.01$). This indicates a consistent co-variability between snow surface and underlying ice surface elevation anomalies at the along-track scale. The nice0201 transect shows a relatively low correlation coefficient ($r = 0.547$), which is likely attributable to its shorter length and limited spatial sampling.

https://doi.org/10.5194/egusphere-2026-4149
Preprint. Discussion started: 15 September 2026

Linear regression analysis further shows that the slopes for different transects are primarily distributed between 0.85 and 1.21. This suggests that the amplitude of snow surface undulations is comparable to that of the underlying ice surface. A few transects exhibit slopes slightly below or above unity, indicating variability in how the snow layer responds to ice surface topography, possibly due to local variations in snow depth, redistribution processes, or differences in transect length. Overall, this correlation analysis provides point-to-point evidence that complements the statistical results presented in Table 1.

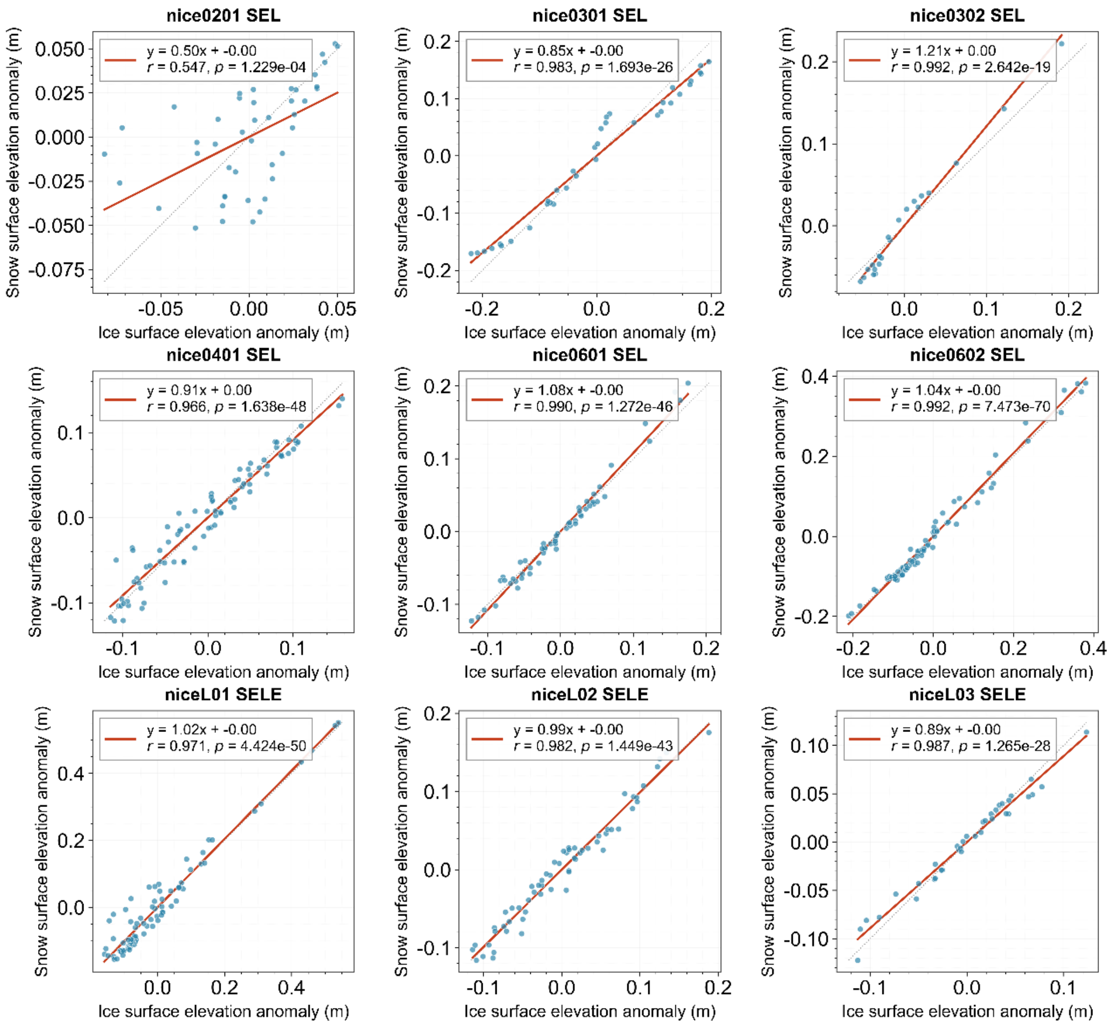

Figure 7. Relationship between ice surface and snow surface elevation anomalies. Each panel corresponds to one transect, with blue dots representing point-to-point matched ice–snow elevation anomalies. The red dashed line indicates the least-squares linear regression, and the gray dashed line denotes the y=x reference line. The Pearson correlation coefficient (r) and its significance level (p-value) are reported in each panel.

https://doi.org/10.5194/egusphere-2026-4149
Preprint. Discussion started: 15 September 2026

3.2 Ice Surface Roughness Characteristics

To quantitatively analyze variations in ice surface roughness across different spatial scales, a multi-scale moving window approach was applied along each RTK survey transect to calculate local surface roughness. Roughness is defined as the standard deviation of ice surface elevation within each window and is calculated along the nine RTK transects. For each sampling point along a transect, all valid observations within a specified window radius centered on that point were selected, and the standard deviation of ice surface elevations within the window was used to represent the local surface roughness. To ensure the robustness of the statistics, only windows containing at least four valid observations were included in the calculation.

Figure 8 shows the relationship between the length-weighted mean ice surface roughness and the analysis window radius, computed from all survey transects. The results indicate a typical scale-dependent behavior of ice surface roughness. As the window radius increases from 2 m to 7 m, the mean roughness rises rapidly from approximately 0.04 m to about 0.065 m, representing an increase of roughly 63%. Within this scale range, roughness is highly sensitive to window size, reflecting the significant contribution of ice surface undulations at these scales.

When the window radius exceeds approximately 10 meters, the roughness continues to increase but at a slower rate. When the window radius is greater than 10 meters, the change in roughness per 1-meter increase in window radius is one-third of that observed when the window radius is less than 7 meters. Although the absolute roughness values vary among different transects, the overall trend of roughness variation with window scale is similar across transects, indicating that the above scale-dependent behavior is generally consistent across different surveyed transects.

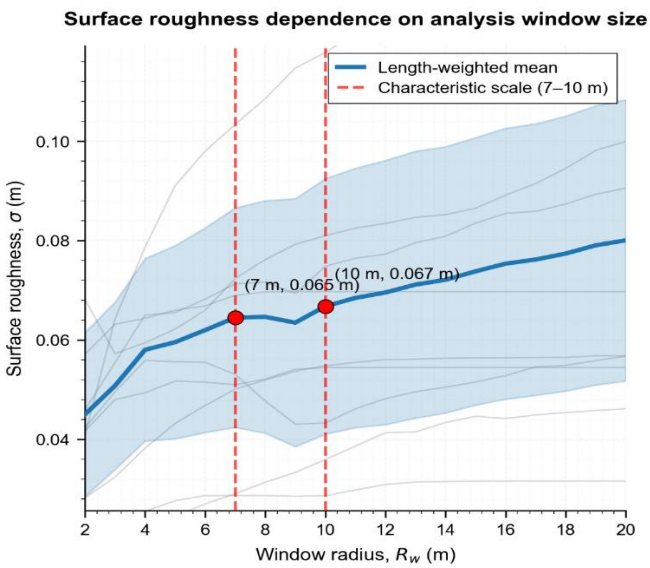

Figure 8. Scale dependence of ice surface roughness as a function of analysis window radius. The dark blue solid line represents the length-weighted mean roughness, the light blue shading indicates the ±1 standard deviation across transects, and the thin gray lines show results for individual transects. The red dashed line marks the characteristic scale (approximately 7 m) at which roughness reaches a relatively stable threshold.

https://doi.org/10.5194/egusphere-2026-4149
Preprint. Discussion started: 15 September 2026

To further examine the correspondence between ice surface and snow surface roughness at the characteristic scale, surface roughness for both ice and snow was calculated along each transect using a window radius of 7 m. All valid window-based estimates were then aggregated for analysis (Fig. 9b). The results show that, consistent with the ice surface elevation anomaly (Fig. 9a), there is a strong positive linear relationship between snow surface roughness and ice surface roughness. The data points are tightly clustered along the regression line, with a Pearson correlation coefficient of r = 0.98, indicating a high degree of statistical consistency between the two.

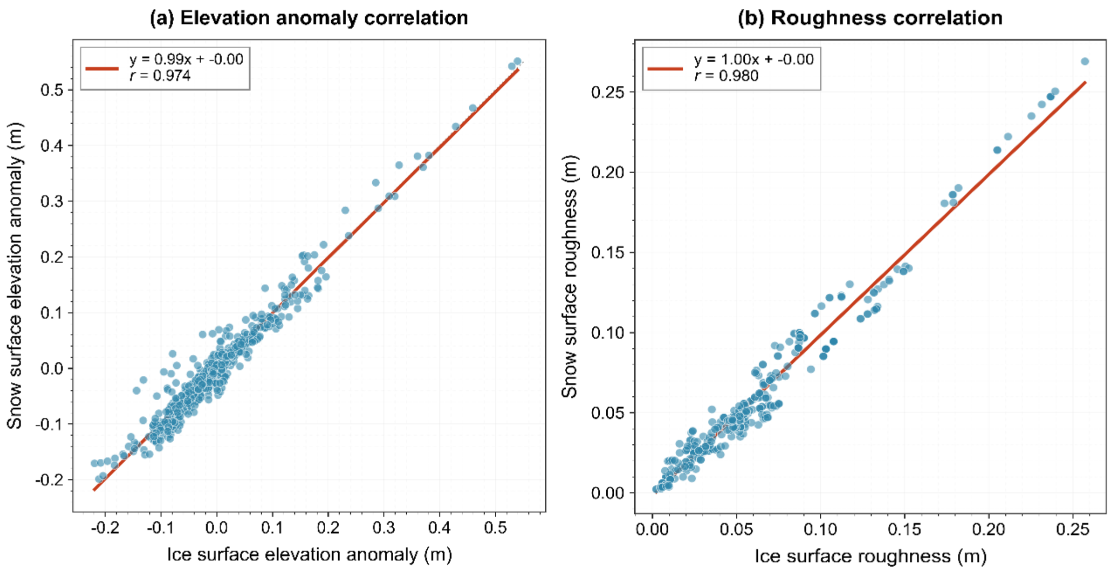

Figure 9. (a) Scatter distribution of ice surface and snow surface elevation anomaly. (b) Scatter distribution of ice surface and snow surface roughness computed using a 7 m moving window. The red solid line denotes the least-squares linear regression.

3.3 Statistical Relationship Between Surface Roughness and Snow Depth

In Sections 3.1 and 3.2, the relationship between snow depth and ice surface morphology was quantitatively examined through amplitude ratio and correlation analyses for geometric consistency (Section 3.1), and a multi-scale moving window approach to characterize the scale-dependent behavior of ice surface roughness (Section 3.2). The results show generally consistent ice–snow elevation anomalies across most transects, with deviations reflecting localized snow redistribution. Building on these findings, this section further quantitatively evaluates the statistical constraint of ice surface roughness on snow depth distribution and examines the sensitivity of this relationship to the spatial scale. Figure 10 presents the variation of the correlation coefficient between ice surface roughness and snow depth as a function of the analysis window radius (Rw). This analysis is based on seven of the nine RTK transects and adopts an adaptive window strategy, in which the maximum window radius for each transect is limited to one-third of its effective length to avoid statistical bias arising from differences in transect length. The two shortest transects, nice0301 and niceL02, both shorter than 250 m, were excluded

https://doi.org/10.5194/egusphere-2026-4149
Preprint. Discussion started: 15 September 2026

from the scale-dependent analysis because their limited effective lengths resulted in insufficient valid moving-window samples at larger window radii.

The correlation curves for individual transects show substantial variability across different window scales, reflecting the spatial heterogeneity of local surface morphology and snow conditions. However, from an ensemble-averaging perspective, all transects exhibit a consistent scale-dependent behavior. Specifically, at small window radii (Rw < 4–5 m), the correlation coefficients are highly scattered across transects, and the overall relationship is weak or even inconsistent in sign, indicating that results at this scale are strongly influenced by measurement noise, local microtopography, and insufficient spatial sampling. As the window radius increases, the correlation between sea ice surface roughness and snow depth strengthens rapidly and converges toward positive values across most transects. The ensemble-averaged correlation reaches a pronounced peak at intermediate spatial scales: the maximum absolute correlation (r = 0.578) occurs at Rw = 8 m, which closely matches the characteristic roughness scale independently identified in Section 3.2. As the window radius further increases to 20 m, the ensemble-averaged correlation remains stable, suggesting that around 8 m marks the lower bound of the characteristic scale at which sea ice surface roughness exerts a significant statistical constraint on snow depth distribution.

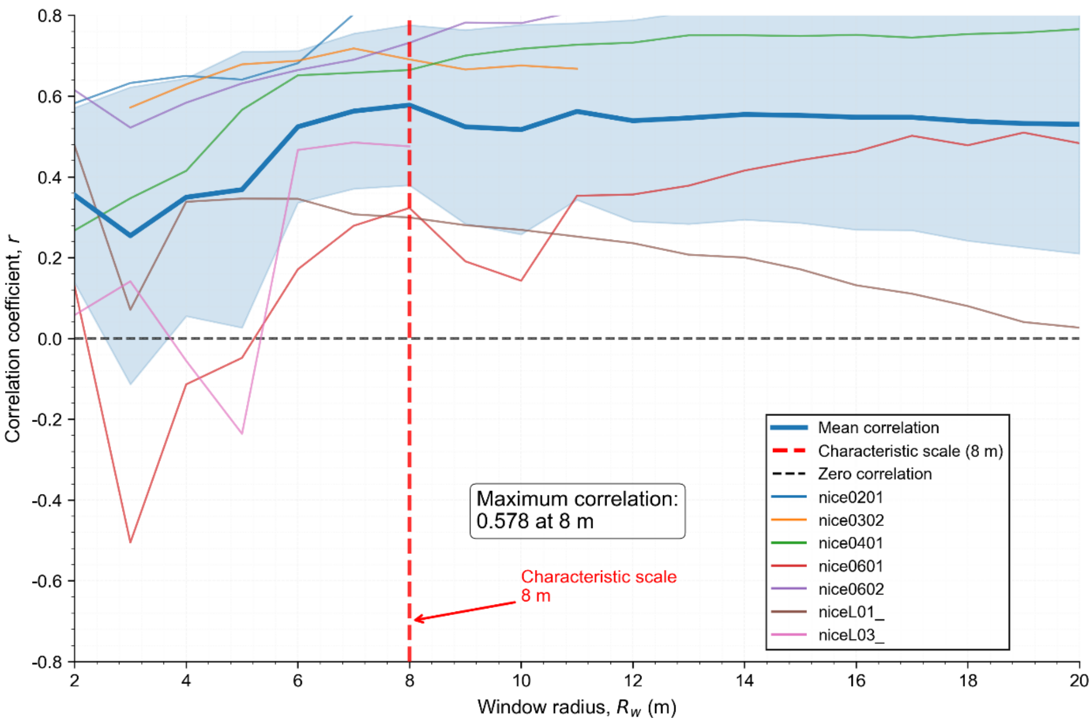

Figure 10. Scale dependence of the correlation coefficient between ice surface roughness and mean snow depth for the RTK transects. The thick blue curve and shaded region indicate the ensemble-mean correlation and standard deviation, respectively. The vertical dashed line marks the characteristic spatial scale of Rw = 8 m, and the horizontal dashed line denotes zero correlation.

Based on the above scale-sensitivity analysis, a window radius of Rw = 8 m was selected to calculate ice surface roughness and mean snow depth. Figure 11 shows the relationship between ice surface roughness and mean snow depth across different

https://doi.org/10.5194/egusphere-2026-4149
Preprint. Discussion started: 15 September 2026

transects at this scale. Surface roughness is defined as the standard deviation of ice bottom elevation within a sliding window of Rw, and mean snow thickness is the average snow depth within the same window (minimum 4 points per window required). For most transects, snow depth increases with increasing ice surface roughness, exhibiting moderate to strong positive correlations ($r \approx 0.3$–0.8). This indicates that, at this spatial scale, larger ice surface undulations favor snow retention and accumulation, likely due to the enhanced resistance of rough surfaces to wind-driven snow transport. For the two shortest transects (length < 250 m), the weak or even negative correlations are likely due to limited sample size. Overall, at the characteristic scale of Rw ≈ 8 m, there is a well-defined statistical relationship between ice surface roughness and snow depth. This scale corresponds to the dominant spatial structure of ice surface roughness itself (Section 3.2), indicating that it has clear physical significance.

https://doi.org/10.5194/egusphere-2026-4149
Preprint. Discussion started: 15 September 2026

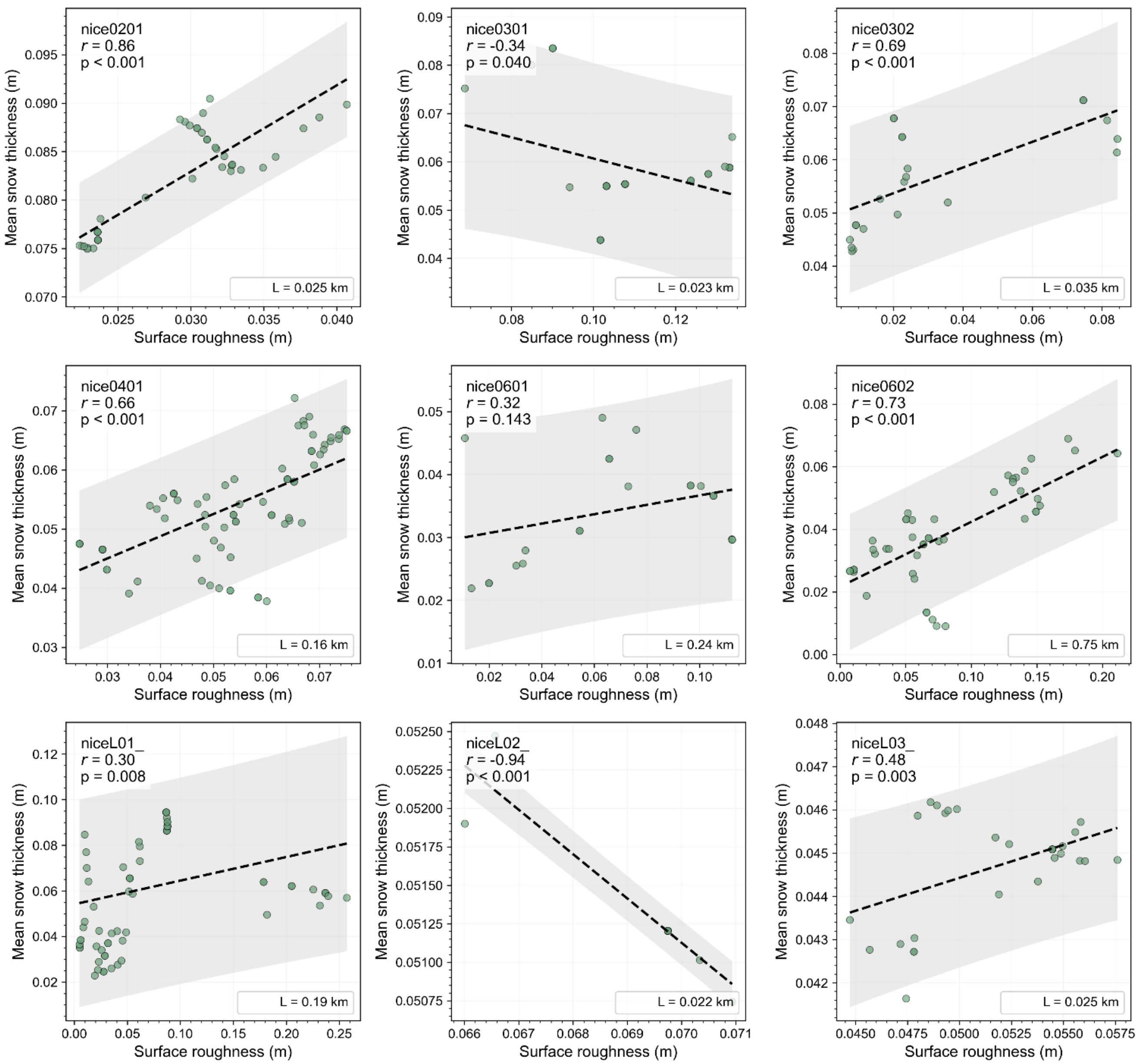

Figure 11. Relationship between surface roughness and mean snow thickness at the characteristic scale (Rw = 8 m). Each panel corresponds to an individual survey track, with track name, number of valid sampling windows (n), Pearson correlation coefficient (r), and corresponding p-value shown in the upper left corner. Track length (L) is indicated in the lower right corner of each panel. The black dashed line represents the ordinary least-squares linear regression, with the shaded area denoting the 95% prediction interval.

4 Conclusion

Based on high-resolution GNSS RTK transect observations collected over multi-year ice in the central Arctic during the 15th Chinese National Arctic Research Expedition in 2025, this study systematically characterizes the spatial coupling between ice surface roughness and snow depth from both geometric and scale-dependent statistical perspectives, and identifies the key spatial scale at which topography modulates snow redistribution. The results show that snow surface elevation anomalies strongly inherit the underlying ice surface topography. While the ice–snow elevation co-variability is strong, deviations in amplitude ratio (e.g., 0.82–1.20) suggest localized smoothing or amplification effects due to preferential snow accumulation or wind-driven redistribution.

In the window scale range of 0 to 20 meters, sea ice surface roughness increases with the window size. Among these scales, a window radius of approximately 7-10 m is identified as the minimum representative scale characterizing the dominant topographic structures, as this scale lies precisely at the transition point where sea ice roughness shifts from rapid increase to gradual increase. This scale may reflect the typical spatial correlation length of surface undulations over multi-year ice, which is also similar to the 5–7 m spatial correlation length of snow depth reported by Kwok et al. (2017). Further scale-sensitivity analysis reveals that the correlation between ice surface roughness and snow depth reaches a maximum at $Rw \approx 8$ m ($r \approx 0.58$) and does not increase further with increasing Rw, indicating that this scale corresponds to the minimum coupling interval at which ice surface topography most effectively modulates snow redistribution. At this scale, rougher ice surfaces are generally associated with thicker snow, reflecting enhanced snow trapping and retention by microtopography. At smaller scales, the relationship is more strongly affected by local noise and limited spatial sampling.

This study also demonstrates that spatial sampling length plays a critical role in the robustness of the roughness–snow depth relationship. Short transects are insufficient to reliably capture the modulation effect of topography on snow redistribution. This finding highlights the necessity of explicitly accounting for the effective scale of surface roughness when developing or evaluating snow redistribution parameterizations in sea ice models, rather than relying solely on empirical relationships at a single resolution. The characteristic scale identified here provides a practical constraint for roughness-controlled snow redistribution processes and offers a physically based reference for the minimum spatial resolution required by remote sensing products to resolve snow heterogeneity.

The integrated GNSS RTK-based observation system developed in this study offers a novel approach to sea ice snow depth measurements. By deploying the base station on drifting sea ice, a local reference frame that moves with the ice is established, and differential positioning effectively removes the effects of ice translation and rotation—solving the spatial mismatch problem caused by continuous ice drift. The rigid integration of snow probes with the RTK rover further enables co-located measurements of snow surface and ice surface elevations within the same reference frame, avoiding systematic biases from instrument switching. With millimeter-level RTK positioning accuracy, the system captures ice and snow surface geometry at meter-to-sub-meter scales, providing a robust observational basis for quantifying the roughness–snow depth relationship and its scale dependence.

https://doi.org/10.5194/egusphere-2026-4149
Preprint. Discussion started: 15 September 2026

5 Discussion

The station configuration spans multiple independent multi-year ice regions, providing a representative observational basis for analyzing sea ice surface roughness, snow depth, and their statistical relationships. The stabilization of ice surface roughness at a scale of approximately 7-10 m implies that roughness statistics at scales larger than this threshold effectively represent the dominant topographic units of multi-year ice, whereas roughness at smaller scales is more susceptible to microtopography and measurement noise. The close agreement between this characteristic scale and the scale (Rw ≈ 8 m) at which the roughness–snow depth correlation peaks suggests that snow redistribution processes primarily respond to terrain variability at this intermediate scale. This consistency provides independent geometric and statistical evidence for the scale-dependent control of topography on snow redistribution.

Most existing sea ice and snow models parameterize snow redistribution using roughness metrics or ridge density, but often lack explicit consideration of the appropriate scale of application. The results of this study suggest that defining roughness at scales significantly smaller than the characteristic scale may overemphasize microscale noise, while defining it at much larger scales may obscure the local control of topography on snow trapping through spatial averaging. Therefore, incorporating roughness parameters at scales of approximately Rw ≈ 8 m may provide a more physically consistent representation of terrain-modulated snow redistribution processes. This characteristic scale also has important implications for the design of remote sensing products targeting sea ice surface roughness. If the effective spatial resolution of a retrieval product is significantly coarser than this scale, it cannot resolve the key roughness elements that control snow redistribution.

Finally, it should be noted that this study focuses on late-summer multi-year ice conditions in the central Arctic. The identified characteristic scale may vary under first-year ice conditions, or different stages of snow evolution. Furthermore, due to the relatively short lengths of the RTK transects, this study could not robustly identify two key scales: (1) the upper bound of the roughness scale dependence, and (2) the scale at which the correlation between ice surface roughness and snow depth begins to weaken. Future work integrating longer transects is needed to extend the observable scale range and to explore potential scale-dependent behavior across different ice types and seasonal conditions.

Code and data availability

The data supporting the findings of this study are available from the corresponding author, Su Jie, upon reasonable request (Email: **sujie@ouc.edu.cn**). Following a two-year confidentiality period, the data will be publicly accessible through the National Arctic and Antarctic Data Center (https://datacenter.chinare.org.cn/).

https://doi.org/10.5194/egusphere-2026-4149
Preprint. Discussion started: 15 September 2026

Author contributions

MW had the concept of the study, processed and analyzed the data, and wrote the draft of manuscript. JS contributed to the concept of the study and participated in discussions of the result. JS and HL deployed the instruments in the field. All authors provided critical feedback and contributed to the editing of the manuscript.

Competing interests

The contact author has declared that none of the authors has any competing interests.

Disclaimer

Copernicus Publications adds a standard disclaimer: “Copernicus Publications remains neutral with regard to jurisdictional claims made in the text, published maps, institutional affiliations, or any other geographical representation in this paper. While Copernicus Publications makes every effort to include appropriate place names, the final responsibility lies with the authors. Views expressed in the text are those of the authors and do not necessarily reflect the views of the publisher.”
Please feel free to add disclaimer text at your choice, if applicable.

Acknowledgements

Data used in this manuscript were produced during 15th Chinese National Antarctic Research Expedition (CHINARE-15). We are deeply grateful to the organizers, crews and scientists onboard the icebreaker R/V Xuelong and R/V Xuelong 2 during the expeditions. We acknowledge the reviewers and the editor for their comments and suggestions

Financial support

This research has been supported by the National Key Research and Development Program of China (grant no. 2023YFC2809101) and the the Laoshan Laboratory Technology Innovation Project (No. LSKJ202202301).

Review statement

The review statement will be added by Copernicus Publications listing the handling editor as well as all contributing referees according to their status anonymous or identified.

References

Itkin, P., Spreen, G., Cheng, B., Doble, M., Girard-Ardhuin, F., Haapala, J., Hughes, N., Kaleschke, L., Nicolaus, M., and Wilkinson, J.: Thin ice and storms: Sea ice deformation from buoy arrays deployed during N-ICE2015, J. Geophys. Res.-Oceans, 122, 4661–4674, https://doi.org/10.1002/2016JC012403, 2017.

Itkin, P., Hendricks, S., Webster, M., von Albedyll, L., Arndt, S., Divine, D., Jaggi, M., Oggier, M., Raphael, I., Ricker, R., Rohde, J., Schneebeli, M., and Liston, G. E.: Sea ice and snow characteristics from year-long transects at the MOSAiC Central Observatory, Elem. Sci. Anth., 11, 00048, https://doi.org/10.1525/elementa.2022.00048, 2023.

King, J., Howell, S., Derksen, C., Rutter, N., Toose, P., Beckers, J. F., Haas, C., Kurtz, N. T., and Richter-Menge, J.: Evaluation of Operation IceBridge quick-look snow depth estimates on sea ice, Geophys. Res. Lett., 42, 9302–9310, https://doi.org/10.1002/2015GL066389, 2015.

King, J., Derksen, C., Toose, P., Langlois, A., Larsen, C. F., Lemmetyinen, J., Marsh, P., Montpetit, B., Roy, A., Rutter, N., and Sturm, M.: The influence of snow microstructure on dual-frequency radar measurements in a tundra environment, Remote Sens. Environ., 215, 242–254, https://doi.org/10.1016/j.rse.2018.05.028, 2018.

Kwok, R., Kurtz, N. T., Brucker, L., Ivanoff, A., Newman, T., Farrell, S. L., King, J., Howell, S., Webster, M. A., Paden, J., Leuschen, C., MacGregor, J. A., Richter-Menge, J., Harbeck, J., and Tschudi, M.: Intercomparison of snow depth retrievals over Arctic sea ice from radar data acquired by Operation IceBridge, The Cryosphere, 11, 2571–2593, https://doi.org/10.5194/tc-11-2571-2017, 2017.

Landy, J. C., Petty, A. A., Tsamados, M., and Stroeve, J. C.: Sea ice roughness overlooked as a key source of uncertainty in CryoSat-2 ice freeboard retrievals, J. Geophys. Res.-Oceans, 125, e2019JC015820, https://doi.org/10.1029/2019JC015820, 2020.

Merkouriadi, I., Liston, G. E., Graham, R. M., and Granskog, M. A.: Quantifying the potential for snow–ice formation in the Arctic Ocean, Geophys. Res. Lett., 47, e2019GL086392, https://doi.org/10.1029/2019GL086392, 2020.

Nab, C., Mallett, R., Gregory, W. K., Landy, J., Lawrence, I. R., Willatt, R., Stroeve, J., and Tsamados, M.: Synoptic variability in satellite altimeter-derived radar freeboard of Arctic sea ice, Geophys. Res. Lett., 50, e2022GL100696, https://doi.org/10.1029/2022GL100696, 2023.

Nandan, V., Willatt, R., Mallett, R., Stroeve, J., Geldsetzer, T., Scharien, R., Tonboe, R., Yackel, J., Landy, J., Clemens-Sewall, D., Jutila, A., Wagner, D. N., Krampe, D., Huntemann, M., Mahmud, M., Jensen, D., Newman, T., Hendricks, S., Spreen, G., Macfarlane, A., Schneebeli, M., Mead, J., Ricker, R., Gallagher, M., Duguay, C., Raphael, I., Polashenski, C., Tsamados, M., Matero, I., and Hoppmann, M.: Wind redistribution of snow impacts the Ka- and Ku-band radar signatures of Arctic sea ice, The Cryosphere, 17, 2211–2229, https://doi.org/10.5194/tc-17-2211-2023, 2023.

Sturm, M., Perovich, D. K., and Holmgren, J.: Thermal conductivity and heat transfer through the snow on the ice of the Beaufort Sea, J. Geophys. Res.-Oceans, 107, SHE 19-1–SHE 19-17, https://doi.org/10.1029/2000JC000409, 2002.

https://doi.org/10.5194/egusphere-2026-4149
Preprint. Discussion started: 15 September 2026

Sturm, M., Maslanik, J. A., Perovich, D. K., Stroeve, J. C., Richter-Menge, J., Markus, T., Holmgren, J., Heinrichs, J. F., and Tape, K.: Snow depth and ice thickness measurements from the Beaufort and Chukchi Seas collected during the AMSR-Ice03 campaign, IEEE T. Geosci. Remote Sens., 44, 3009–3020, https://doi.org/10.1109/TGRS.2006.878236, 2006.

Webster, M. A., Rigor, I. G., Nghiem, S. V., Kurtz, N. T., Farrell, S. L., Perovich, D. K., and Sturm, M.: Interdecadal changes in snow depth on Arctic sea ice, J. Geophys. Res.-Oceans, 119, 5395–5406, https://doi.org/10.1002/2014JC009985, 2014.